Fire Performance of Steel Profiles Covered with Self Compacting Concrete

Abdulkadir Cüneyt AYDIN[a*], Bariş BAYRAK[a], Haluk Gorkem ALCAN[b], Mahmut KILIÇ[a], Mahyar MAALI[c]

[a]Ataturk University, Engineering Faculty, Department of Civil Engineering, Erzurum, TURKEY.
[b]Kafkas University, Faculty of Engineering and Architecture, Department of Civil Engineering, Kars, TURKEY.
[c]Erzurum Technical University, Faculty of Engineering and Architecture, Department of Civil Engineering, Erzurum, TURKEY.
[*]Corresponding Author: Tel: +90 442 231 48 51
Phone Number: +90 530 678 61 61
E-mail: acaydin@atauni.edu.tr
E-mail addresses: bbayrak@kafkas.edu.tr (Baris Bayrak), hgorkemalcan@kafkas.edu.tr, mahmut.kilic@atauni.edu.tr (Mahmut Kılıç), mahyar.maali@erzurum.edu.tr (Mahyar Maali)

Abstract

This paper reports an investigation on the high-temperature effect on the composites manufactured with steel profiles embedded within the concrete for varying temperatures. A total of 24 experiments were performed in two groups and all specimens were manufactured with self-compacting concrete. The effects of high temperature are investigated through rectangular prism type specimens, by using the concrete cover as 25, 50, and 75 mm. The testing temperatures were kept constant for each group (600 ℃ and 900 ℃). The effects of varying exposure time (60 and 120 minutes) on the relevant steel standard IPE profiles (IPE 120 and IPE 270) were experimentally investigated. Furthermore, the micro structure of the composite is observed by using scanning electron microscopy (SEM) technique. The increase in the concrete cover in both groups increased the compressive strength. Increasing the concert cover allowance decreased the crack distribution and maximum crack width. However, concrete cover, high temperature and exposed time have a significantly effect on the yield strength and ultimate strength of IPE profiles.

Keywords: I-profile; Concrete cover; High temperature; Self-compacting concrete; Composite.

1. Introduction

The steel and concrete are the main structural materials of construction technology, not only used separately, but also used together as composite. Today, steel tubes and embedded steel sections are often used as composite columns and beams in high-rise buildings, large-span factories, etc. The combined use of concrete and steel both increases the load-bearing capacity of the structure and provides protection against elevated temperatures. When the I-section steel embedded in the composite beam or column is exposed to

fire, the concrete, which covers that steel, retards the temperature increase in the embedded steel due to its low heat conduction coefficient. Covering embedded steel with concrete provides an insulating layer and it can also significantly increase the load-bearing capacity if reinforced appropriately. Therefore, the overall fire resistance of columns, beams and shear walls can be improved with concrete without any external fire protection [1-12]. The fire behavior of structural composite elements is one of the key design parameters. Hence, the researchers have focused on the both experimental and numerical investigations of the fire and post-fire behavior of composite structural elements [13-15]. On the other hand, the fire accidents may cause to significant damage of structural element such as steel-concrete composite columns or shear walls [16-19]. Some experimental studies on the fire resistance of composite concrete were published. The following ones are a summary of them. Ellobody and Young [20] investigated fire resistance of the columns with different cross-sectional area, different-sized steel profiles, varying aggregates, various load levels. By using the 3D finite-element method, the interface bond between the steel and the concrete is examined. The concrete in contact with the full surface of the steel profile made a good bond. The concrete around the profile made a bond, and the concrete on the outer surface was called non-bonded concrete. The columns with cross-sections of 25x25, 30x30, 35x35, and 40x40 cm^2 were produced. The aggregates used were granite, marble and limestone. While the temperature arises to 900 ℃, the applied load ratios were 0.3 and 0.5. Mao and Kodur [21] investigated the column size, temperature exposure from three or four sides, the load density and load eccentricity. The data obtained from the experiment were used to investigate the effect of concrete coated steel columns on the structural and thermal effects. Until now, fire resistance of structural elements under constant load was observed. However, these elements were subjected to eccentric loads, as in the real life, in this study. The cross-sectional area was constant 35x25 cm^2 and the heating furnaces up to 1200 ℃. Li et al. [22] examined the exposure strength of the buried reinforcement bar at varying temperatures (200, 400, 600, 800 ℃) for 2 hours. The heated specimens were cooled by air and water and their mechanical properties were examined. Wei et al. [23] are carried out the fire resistance of the wall. In the experiments, the temperature was given uniformly for 2 hours and unilaterally for 2.5 hours. Thus, the number of surfaces on which the temperature effects are also observed. These experiments were carried out in heating cabinets up to 1000 ℃. Kaffash et al. [24] have investigated to the fire behavior of mentioned structural system under several fire conditions. The results have been showed that to exposure the high temperature resulted to decrease the lateral resistance of stories. Epackachi et al. [25] conducted on a numerical study to investigate the 3D nonlinear finite element analysis for a floor of high

building under fire scenario. Based on results of the numerical analysis, the connection rapture and collapse of girders led to collapse of the structure. Anvari et al. [9] have carried out a numerical study to investigate the behavior of concrete-filled composite plate shear walls subjected to combined gravity and fire loading. Continued fire exposure led to crushing/global instability failure of walls under gravity loads. The time to failure of the walls reduced considerably with a reduction in rotational fixity at the boundary conditions, reduction in wall thickness, and an increase in the wall slenderness. Yang et al. [26] strength, deformation and ductility parameters of columns with I-profile were investigated after exposure to heat. It was found that the increase in the temperature time that the composite columns are exposed to the temperature decreases the strength. Yang et al. [27] have been carried out a numerical and analytical investigation about the composite frame with the tubed-reinforced-concrete columns under the fire. They have suggested an approach to consider the continuity and interactions between structural elements within a composite frame for the tubed-reinforced-concrete columns under fire. Li et al. [28] carried out a numerical investigation to propose to estimate the mechanical behavior of concrete filled steel tubular columns under fire conditions. They have proposed a theoretical formulation to estimate the ultimate bearing capacity of columns. So, the aim of this study is to investigate the effect of varying concrete cover (25, 50 and 75 mm), varying temperature (600 ℃ and 900 ℃), and varying exposure time (60 min and 120 min) on the relevant steel standard IPE profiles (IPE 120 and IPE 270), which will be mentioned throughout this work as I profile. The 28-day compressive strength of the samples exposed to heat was tested. The effect of curing conditions in air and water on the compressive strength was investigated. In addition, the samples were taken from I120 and I270 profiles that covered with concrete, and the tensile test was applied. The SEM images were evaluated to investigate how the added mineral additives affect the CSH structure of the concrete and to examine I-profile interface bond used.

2. Experimental program

In this study, fire resistance of the most-used steel I profile in the construction sector is examined. Thus, a total of 24 experiments were performed in two groups which these groups are the I120 and I270 (S235) profiles. The cross-sectional dimensions of IPE120 and IPE270 profiles are in accordance with steel standards and the length of all samples is fixed as 300 mm. The experimental symbolization is as designed as Ix-Cy-Tz-tm (I: IPE standard profile, C: concrete cover, T: temperature degree and tm: the minute of temperatures). In order to observe the effect of steel profiles under temperature experimentally, 25 mm, 50 mm and 75 mm concrete cover, which are used the most frequently in columns, beams, walls

and foundations were preferred. Since the average extinguishing time of a fire in a building varies between 60 and 120 minutes [22, 23], the steel profiles embedded in the concrete are exposed to relevant temperatures for 60 and 120 minutes. According to relevant literature mentioned above, the testing temperatures are decided as 600 ℃ and 900 ℃ within this study. Therefore, it is important to what extent the steel profiles are affected by the temperature during these periods. **Figure 1** and **Table 1** show the specimens, and the details of the experimental tests.

Self-compacting concrete (SCC) was used in the study to allow the concrete easily to settle in the mold with its own weight. The SCC technology has a few advantages because of good workability under the own weight in the concrete industry. To achieve the required workability, the fine aggregates and super plasticizer were chosen in the mixture. However, the smaller maximum aggregate size should be used in SCC mixture compared to conventional concrete (CC). By using super plasticizer, it is aimed to prevent creep and shrinkage cracks that occur over time. However, the workability of SCC was increased by using filler and fly ash [29-31].

The construction sector in the world has been used widely 30 MPa for concrete (compressive strength for 28-days). The compressive strength and the SCC mix were kept constant in all samples. The SCC mixes with fly ash were produced by using the Portland Cement (CEM I 32.5). **Table 2** shows the chemical properties of Portland Cement and fly ash.

The maximum aggregate size was 16 mm. In concrete casting, the fine and coarse aggregates, firstly, were mixed for three minutes with cement and fly ash. After that, the super plasticizer (Daracem 200) and 1/3 of water were added to the mixture and mixed for a further 1 minute. At last, 2/3 of the water were added and mixed for a minute, again. The details of the concrete mixture were shown in **Table 3.**

Fresh concrete tests were carried out after mixing the materials. The results of the tests are important for determining the rheological properties of SCC. The viscosity of the concrete influence the flow rate of the SCC. In addition, SCC must have four main features, these can be sorted as follows: First, it must fill the mold in which it is poured with its own weight. Second, aggregate grains should not be over-segregated. Another feature of the SCC should have been that it can pass through gaps between rebar’s. Finally, after demolding, surfaces of the concrete samples should be smooth. These main features are determined by the V-funnel flow time, visual stability index, slump flow time and diameter, L-box and J-ring tests. Detailed information about these tests is contained in the ASTM [32], EFNARC [33] and ACI 237R [34] standards. Some researchers have determined that slump flow time and diameter tests can be used for the flow property of concrete on the

horizontal surface. For slump flow time testing, fresh concrete is filled into the slump cone on a flat surface. After the cone is lift up, the time during which the concrete spreads to a diameter of 500 mm is the time of the slump flow (t_{50}). In addition, the largest diameter in which concrete spreads is the slump flow diameter. L-box is another test carried out to fresh concrete and this test is performed to observe the ability of self-compacted concrete to flow through its reinforcing bars without segregation. L-box test has two kinds, these are two-bar and three-bar tests. Three-bar test was chosen in this study to represent more congested reinforcement range. Fresh concrete is placed in the vertical hopper of L-box and then the slide gate is opened. Lifting the slide gate allows the concrete to flow past the bars into the horizontal trough. The final depth of the concrete at the gate (H_1) and at the end of the trough (H_2) is measured and the proportional difference (H_2/H_1) expressed as a blocking ratio [35-42]. In this study, L box, and V funnel experiments were performed to determine the fluency of SCC. The results of thesee experiments for SCC are shown in **Table 4.** The fresh concrete, hardened concrete, L box and V funnel tests are presented in **Figure 2.**

In order to decide the concrete compressive strength, the poured 150x150x150 mm cube samples were crushed after 90 days. All other test results were made on the 90th day, when the concrete strength gained approximately 99% of its strength. In addition, the cube samples were cured in air and water for a better interpretation of the test results, and the compressive strength of 90 days was examined.

The specimens were first heated to 600 ℃, and 900 ℃ over 60 and 120 minutes in a furnace, as illustrated **Figure 3**, after the air curing process for 90 days. Then, heating was stopped, and the furnace began to cool down slowly until it reached the ambient temperature. However, the specimens were exposed to temperature according to the ISO 834 [43] fire standard to evaluate the behavior of the concrete cover, temperature, exposure time and profile type. Comparison of the ISO with the experimental temperature-time curve is shown in **Figure 4.** It can be seen from **Figure 4** that the experimental and the standard data are very close to each other and the temperatures of 600 and 900 degrees, which are the parameters of the study, are marked on the curve. The experimental temperature-time curve was plotted using the formula $T=20+345\log_{10}(8t+1)$, where T is temperature in furnace (^{o}C) and t is the time (minute).

3. Results

Table 5 shows that the cube samples (150x150x150 mm) without I Profile were cured in air and water for a better interpretation of the test results and the compressive strength of 90 days. **Table 5** shows a decrease in compressive strength of samples exposed to fire

for all. In fact, to compare to control sample, exposure to 900 ℃ for 2 hours caused the compressive strength a decrease about 84.76% and 87.01% for samples with air cured and water cured, respectively. In addition, although the temperature exposure time was increased for the samples exposed to 600 ℃, the decrease in compressive strength was very small. However, when the temperature to which the samples are exposed increases from 600 ℃ to 900 ℃, the difference in strength between water and air cured one is quite high. It has been experimentally observed that the damage of the concrete samples exposed to 600 ℃ temperature is repairable. However, when the temperature rises to 900 ℃, the damage in the concrete is irreparable.

Xiong and Liew studied the fire resistance of ultra-high strength concrete. As a result of their tests, they found that the compressive strength of the concrete decreased by about 70% at 800 ℃ [44]. Also researchers noted that the elevated temperature reduced the compressive strength of concrete by 25% at 400 ℃, 32-38% at 600 ℃, 63-77% at 800 ℃, and more than 85% at temperatures above 900 ℃ [45-47]. In addition, research has shown that the compressive strength of air-cured concretes is lower than that of water-cured concretes [48-51].

3.1. Concrete Related Results

Table 6 and **Figures 5**, shows the concrete compressive strength of specimens. Concrete compressive strength values were obtained by applying the uniaxial compressive strength test to 50x50x50 mm cubes according to the ASTM C109 standard [52]. 50x50x50 mm cubes were removed from the insides of the samples that were exposed to heat. The increasing in the concrete cover in both groups increased the concrete compressive strength. In the I270 group, the highest increase was obtained in the T600-t120 sample about 281% and in the I120 group, the highest increase was obtained in the T900-t60 sample about 158%. In **Figure 5**, the increase in temperature exposure time decreased the concrete compressive strength. Nevertheless, the compressive strength of C75-T900-t120 sample of I270 group was higher than that of C25-T900-t60. This shows that the cover of concrete and steel composite elements exposed to temperature has an important effect on the concrete compressive strength. A similar situation can be seen in **Figure 5** although the C75-T600-t120 sample was exposed to the same temperature but more time than the C25-T600-t60 sample with 393% higher compressive strength. The temperatures to which the samples are exposed during the same period are different. It is already expected that the concrete compressive strength will decrease with the increase of the exposed temperature value, but the decrease of the compressive strength in the concrete decreases considerably when the time of exposure to heat doubles.

The concrete compressive strength for I120 and I270 groups were shown in **Figures 5**. However, the temperature increase from 600 degrees to 900 degrees in samples exposed to 2 hours temperature with 75 mm concrete cover decreased the concrete compressive strength by 324%. In general, **Table 6**, shows the increase in profile cross-section in both groups (using I270 instead of I120) has a little effect on the concrete compressive strength.

As expected, the **Figure 5** implies the positive effect of increasing cover, decreasing heating temperature, and time on the compressive strength of the samples. However, the volume of the samples varies, the area of the profile increases, too. The incremental effect of volume change including size effect can be seen for both rows of the **Figure 5**. The effective volume of concrete increased about three times while the steel volume is increased about 3.5 times. Thus, heat absorbability of the steel increased the negative effect of heating time on the compressive strength, by relative elongation of the heating time. Furthermore, the width of profiles heading also increased the observed cracks throughout the surface of the specimen, which were decreased at flange related surface. The increased cover depth was the second main effect of crack propagation at the profile heading related surface, which also decreases the crack width. Nevertheless, the crack numbers increased with increasing profile.

3.2. Steel Profiles Related Results

The stress-strain curves of steel were drawn to evaluate the post fire behavior. The samples to be subjected to the uniaxial tensile test were cut from the midpoints of the I120 and I270 profiles. The dimension of samples was prepared in according to the ASTM E8 standard [53]. The before and after photos of samples were shown in **Figure 6.**

The tensile tests were carried out displacement control with a constant speed of 0,04 mm/sn. The stress-strain curves are shown in **Figure 7**. The observed and evaluated test results are presented in **Table 7**. **Table 7** shows that the E (Elastic modules), f_y (yield stress), f_u (ultimate stress), ε_y (yield strain), ε_u (ultimate strain) and the area under the stress-strain curve decreased with increased time of heating for the same model with same characteristics for both groups. The area under the stress-strain curve is a sign of energy dissipation capacity of the member/model/specimen. Also, the E, f_y, f_u, ε_y, ε_u and the area under stress-strain curve for 600 ^{0}C are greater than the ones for 900 ^{0}C. Thus, the temperature plays a significant role for the E, f_y, f_u, ε_{uni}, ε_f, and energy adsorption capability, for the steel-concrete composite structures. The energy adsorption capability, which is also a sign of ductility and/or toughness, is increased with increasing steel section by using greater sections of I-type

profiles, as seen in **Table 7,** as expected. This implementation is also can be widened for the E, f_y, f_u, ε_y, ε_u values for unaffected profile sections for two hours.

The highest E values in I270 and I120 groups were obtained in I270-C50-900-60 and I120-C75-T900-t120 specimens, respectively. In addition, the E value of the I120-75-T900-t120 sample is 9.70% higher than that of the I270-C50-T900-t60 sample. As expected, the increase in the time of exposure to temperature decreased the modulus of elasticity in all other specimens. Increasing the exposure time to temperature increased the modulus of elasticity, as a result of heating sensitivity and conductivity of the steel. I270-C50-T600 is the group in which the exposure time to heat affects the elasticity modulus the most. Doubling the time in this group decreased the modulus of elasticity by 24.96%. The least effect was that doubling the temperature in the I270-C50-T900 sample decreased the modulus of elasticity by 3.08%. E value of I120-C75-T900-t120 sample is 55.21% higher than I120-C75-T900-t60. In I270 and I120 groups, the highest yield strengths were reached in I270-C25-T600-t120 and I120-C25-T600-t60 specimens, respectively. Increasing the temperature decreased the yield strength in both I270 and I120 groups, as expected. Similarly, increasing the exposure time to temperature decreased the yield strength in general. In the I270-T600 group specimens, an increase in the concrete cover from 25 mm to 50 mm decreased the yield strength, but an increase in the concrete cover from 50 mm to 75 mm increased the yield strength. In the I270-T900 group, the increase in the concrete cover (from 25 mm to 75 mm, respectively) caused the yield strength to increase first and then to decrease. When the I270 and I120 group specimens with the same properties are compared, the yield strength values of all the I270 group specimens were found to be higher than the I120 group specimens. In the ultimate yield strength values of I270 and I120 groups, the highest results were obtained in I270-C50-T900-t120 and I120-C25-T600-t60 specimens, respectively. Changing the profile type had an effect on the ultimate yield strength. Increasing the profile cross-sectional area (I270 group) increased the ultimate yield strength. Also, increasing the temperature exposure time generally decreased the ultimate strength in all samples except a few samples.

The microstructure of the iron/steel enhanced the conductivity and movability of the electrons throughout their expected positions to a wider range, which gets the yielding point lower in related to relevant yielding testing temperature standards, also. The constantness of the elastic modulus also, visualized for similar temperatures, while the increasing temperature enhanced the ability of deformation for the steel samples at **Figure 7**, as expected. However, the increasing temperature negative effects were implied itself at stress rate. Withal, the mostly protected steel samples

with greater cover thickness, enhanced the expecting behavior of the steel samples.

The mechanical properties of structural steel exposed to high temperature vary depending on its many properties. Many studies have been conducted on the effect of structural steel on the change of mechanical properties of its microstructure, size or cross section, fire protection layer, cooling method, temperature rating and temperature duration [54-58].

In **Figure 8**, the energy dissipation capacities of the tensile tested samples were calculated. The energy dissipation capacity was calculated from the areas under the stress-strain graphs drawn after the tensile test. The energy absorption capacities of I270 profiles generally are higher than I120 profiles. The highest and lowest energy dissipation capacities were obtained in I270-C25-T600-t120 and I120-C50-T900-t120 samples, respectively. Profile type, concrete cover, exposure time and temperature significantly affected the energy dissipation capacity of the samples. The increase in the concrete cover caused the profiles in the concrete to be less affected by the temperature. So, less damage occurred under temperature. Therefore, the increase in the concrete cover also increased the energy dissipation capacity. The crack widths were less with the decrease in temperature and exposure time to heat. Therefore, the profiles in the concrete were less affected by the temperature and the energy absorption capacity was higher.

3.3. Failure

The **Figures 9a and b** show, the crack formation and distribution were similar when the both I120 and I270 groups doubled the exposure time for 900 ^{0}C. Furthermore, **Figure 9** shows, increasing the concrete cover allowance decreased the crack intensity and the maximum crack width. Similarly, it was experimentally observed that increasing the temperature affected the crack intensity and the crack width. The crack distribution was similar for all test samples; in the surface, the cracks progressed downwards and horizontally on large surfaces. The cross-section of the composite member, also affected the crack width as an increase, as can be seen in **Figure 9**. The crack distribution was similar in both I120 and I270 groups; the cracks propogated horizontally on the narrow edges of the specimens and downward on the wide edges. The increasing the cover concrete content in the I270 group did not have much effect on the crack distribution at the high temperatures (900 degrees). In the I120 group, cover concrete content was more effective on the crack mechanism of the samples. However, doubling the temperature exposure time at 900 degrees increased the maximum crack width, as expected.

The cracks at the surface, which were decreased are presented a similar trend at the flange-related surface, which also implied

itself by decreasing crack width but increasing crack numbers. The crack distribution of the samples exposed to fire, Xiao et al. [59] divided the cracks formed in the samples after the fire into three groups. In the first group, they stated that there is only one main crack in the axial direction. In the second group, several cracks form and develop in the axial direction while in the third group, a lot of cracks form and develop catastrophically. The cracks in this study (**Figure 8**) were formed as in the first and second groups. The cracks of the samples produced with the I120 profile were generally formed and developed as first group cracks. In the samples produced with the I270 profile, the second group of cracks was observed.

3.4. Scanning electron microscope (SEM) results

The reason for using SEM in this study is to observe how the added mineral additives affect the CSH structure of the concrete and to examine I-profile interface bond used. The Zeiss Gemini SEM device used for image acquisition. The voltage range that this device can display is 0.2-30 kV. **Figure 10 and 11** show some experimental tests related steel and concrete SEM images after heating process.

The main behavior of the cement-based composites is related with the hydration process of cement and water. Thus, the water movement will affect the mechanical and durability properties, also. Especially, the increasing temperature will greatly vitiate the calcium silicate hydrate gel and calcium hydroxide. The further increase of the temperature will also result from decomposition of these components. Many researchers have been investigated the behavior of cement-based composites and reported in the literature [23-30].

The SEM graphs are presented at **Figure 10**, to show the microstructure evaluation by increasing time and temperature for the concrete samples. Furthermore, the water and air cured only concrete samples are separately appended to the testing groups. The morphological variation of calcium silicate hydrate gel, the microcracks, and ettringites etc. are visualized, with SEMs, as an extensive way. The surface topography indicates the microstructure change. Especially, by increasing temperature, the number of voids and microcracks; and also, the microcrack width increase are as seen in **Figure 10.** Furthermore, the decomposition of calcium silicate hydrate gel is very visible at **Figure 10c**. The **Figure 10g, h, and i**, also demonstrate the disintegration of calcium silicate hydrate gel. Moreover, the microcrack propagation through interface layer and calcium silicate hydrate gel are very attractive at **Figure 9a and i,**

respectively. The predominance of microcracks increased the porosity and therefore the loss of strength (**Table 6** and **Figure 10**).

The SEM microstructures of steel profiles are presented in **Figure 11**. As seen, the perlitic microstructure of the steel profiles proves the microstructural behavior. While the carbon-rich cementite phase is dark, the ferrite phase shows itself with lightness. This interlammer spacing gets wider by the temperature increase, which means the rigidity loss of the member. The toughness is related with the crystallographic grain size, represented by colony size. However, the mentioned strength loss can be meaning full for the samples presented in **Figure 101, c, e, and f,** which are delayed 120 minutes for 900 ^{0}C. The fine precipitates are increased after heating temperature increase with increasing dislocation density, also. This precipitation strength proves the high temperature strength of the steel. The martensite-austenite phases can be seen in **Figure 11f** as small islands, especially. Furthermore, the concrete cover did not show a meaningful effect by changing the concrete type from C25 to C50 or C75; all concrete types acted as expected fire guard within the same manner.

4. Conclusion

The aim of this study is to investigate the effect of varying concrete cover (25, 50 and 75 mm), varying temperature (600 and 900 ℃), and varying exposure time (60 and 120 min) on the relevant steel standard IPE profiles (IPE 120 and IPE 270), which will be mentioned throughout this work as I profile. In this study, 24 samples were implemented to investigate the effect of varying concrete covers (25, 50 and75 mm), temperatures (600 and 900 ℃), and exposure times (60 and 120 min) on IPE profiles (I120 and I270) of different lengths embedded in concrete. Some additional results that can be learned from this study are as follows:

1- The increase in the cover concrete in both groups increased the concrete compressive strength. So, the cover of concrete and steel composite elements exposed to temperature has a significant effect on the compressive strength of concrete.
2- It is already expected that the concrete compressive strength will decrease with the increase of the exposed temperature value, but the decrease of the compressive strength in the concrete decreases considerably when the time of exposure to heat doubles.
3- The temperature increases from 600 degrees to 900 degrees in samples exposed to 2 hours temperature with 75 mm concrete cover decreased the concrete compressive strength by 324%. In general, the increase in profile cross-section in both groups

(using I270 instead of I120) has a little effect on the compressive strength of concrete.

4- The E, f_y, f_u, ε_y, ε_u and energy dissipation capacity decreased with increased minute temperature of the same model with same characterizes in the two groups.
5- The E, f_y, f_u, ε_y, ε_u and energy dissipation capacity values of test with 600-degree temperature are bigger than tests with 900-degree temperature.
6- The E, f_y, f_u, ε_y, ε_u and energy dissipation capacity increased with increased I-section steel. Thus, in any such instrument, the large profile section will maintain its original profile in temperature in the 120 minutes.
7- Increasing the cover concert allowance decreased the crack distribution and maximum crack width. Similarly, it was experimentally observed that increasing the temperature affected crack distribution and crack width. The crack distribution was similar for all test samples; in the surface, the cracks progressed downwards and horizontally on large surfaces.

Declaration of Conflict of Interests

The authors declare that there is no conflict of interest. They have no known competing financial interests or personal relationships that could have appeared to influence the work reported in this paper.

Ethical approval: This article does not contain any studies with human participants or animals performed by any of the authors.

References

[1] Han, L.H., and Huo, J. "Concrete-filled hollow structural steel columns after exposure to ISO-834 fire standard" *Journal of Structural Engineering*, **129**(1), pp. 68-78 (2003).

[2] Han, L.H., Huo, J., and Wang, Y.C. "Compressive and flexural behaviour of concrete filled steel tubes after exposure to standard fire" *Journal of Constructional Steel Research*, **61**(7), pp. 882-901 (2005).

[3] Han, L.H., Zhao L.H., Yang, X.L., et al. "Experimental study and calculation of fire resistance of concrete-filled hollow steel columns" *Journal of Structural Engineering,* **129**(3), pp. 346-356 (2003).

[4] Tan, K.H., and Tang, C.Y. "Interaction model for unprotected concrete filled steel columns under standard fire conditions" *Journal of Structural Engineering*, **130**(9), pp. 1405-1413 (2004).

[5] Lie, T. T., and Martin C. "A method to predict the fire resistance of circular concrete filled hollow steel columns" *Journal of Fire Protection Engineering,* pp. **2**(4), pp. 111-124 (1990).

[6] Sakumoto, Y., Okada, T., Yoshida, M., et at. “Fire resistance of concrete-filled, fire-resistant steel-tube columns”, *Journal of Materials in Civil Engineering*, **6**(2), pp. 169-184 (1994).

[7] Yang, D., Liu, F., Huang, S.S., et al. “Structural behaviour and design of end-restrained square tubed-reinforced-concrete columns exposed to fire”, *Journal of Constructional Steel Research,* 182, pp.106675 (2021).

[8] Xie, Q., Xiao, J., Xie, W., et al. “Cyclic tests on composite plate shear walls–concrete encased before and after fire exposure”, *Advances in Structural Engineering,* **22**(1), pp. 54-68 (2019).

[9] Anvari, A.T., Bhardwaj, S.R., Sharma, S., et al. “Performance of composite plate shear walls/concrete filled (C-PSW/CF) under fire loading: A numerical investigation”, *Engineering Structures*, 271, pp. 114883 (2022).

[10] Masoumi-Zahaneh, F., Hoseinzadeh, M., Rahimi, S., et al. “Numerical investigation of buckling-restrained steel plate shear wall under fire loading”, *Earthquakes and Structures*, **23**(1), pp. 59-73 (2022).

[11] Xiong, Y., Chen, A., Wu, D., et al. “Seismic performance of composite shear walls filled with demolished concrete lumps and self-compacting concrete after fire”, *Buildings*, **12**(9), pp. 1308 (2022).

[12] Hosseinpour, M., Celikag, M., and Akbarzadeh, B.H. “Strengthening and shape modification of fire-damaged concrete with expansive cement concrete and CFRP wrap”, *Scientia Iranica*, **26**(2), pp. 699-708 (2019).

[13] Liu, F., and Wang, Y., Gardner, L., et al. “Experimental and numerical studies of reinforced concrete columns confined by circular steel tubes exposed to fire”, *Structural Engineering,* **145**(11), pp. 04019130 (2019).

[14] Yang, D., Liu, F., Huang, S.S., et al. “ISO 834 standard fire test and mechanism analysis of square tubed-reinforced-concrete columns”, *Journal of Constructional Steel Research,* 175, pp. 106316 (2020).

[15] Mirzaei, P.P, and Gerami, M. “Collapse assessment of protected steel moment frame under post-earthquake fire”, *Scientia Iranica*, **27**(6), pp. 2775-2789 (2020).

[16] Yang, D., Liu, F., Huang, S.S., et al. “Structural fire safety design of square and rectangular tubed-reinforced-concrete columns”, *Structures*, pp. 1286-1321 (2021).

[17] Liu, F., Yang, H., Yan, R., et al. “Experimental and numerical study on behaviour of square steel tube confined reinforced concrete stub columns after fire exposure”, *Thin-Walled Structures*, 139, pp. 105-125 (2019).

[18] Nan, Z., Dai, X., Chen H., et al. “A numerical investigation of 3D structural behaviour for steel-composite structures under various travelling fire scenarios”, *Engineering Structures*, 267, pp. 114587 (2022).

[19] Bastami, M., Bastami, A.C., Baghbadrani, M., et al. “Performance of high strength concretes at elevated temperatures”, *Scientia Iranica,* **18**(5), pp. 1028-1036 (2011).

[20] Ellobody, and Young E.B. “Investigation of concrete encased steel composite columns at elevated temperatures”, *Thin-Walled Structures*, **48**(8), pp. 597-608 (2010).

[21] Mao, X., and Kodur, V. “Fire resistance of concrete encased steel columns under 3-and 4-side standard heating”, *Journal of Constructional Steel Research,* **67**(3), pp. 270-280 (2011).

[22] Li, X., Bao, Y., Xue, N., et al. “Bond strength of steel bars embedded in high-performance fiber-reinforced cementitious composite before and after exposure to elevated temperatures”, *Fire Safety Journal*, 92, pp. 98-106 (2017).

[23] Wei, F., Fang, C., and Wu, B. “Fire resistance of concrete-filled steel plate composite (CFSPC) walls”, *Fire Safety Journal*, 88, pp. 26-39 (2017),

[24] Kaffash, M., Karamodin, A., and Moghiman, M. “Behavior of concentrically braced steel frames under fire loading”, *Scientia Iranica*, **29**(3), pp. 951-963 (2022).

[25] Epackachi, S., Mirghaderi, S.R., and Aghelizadeh, P. “Failure Analysis of the 16-Story Plasco Building under Fire Condition”, *Scientia Iranica* (2022).

[26] Yang, H., Yang, X., and Mao, Z. “Compressive performance of steel-reinforced concrete columns after exposure to high temperature”, *Journal of Building Engineering*, 59, pp. 105120 (2022).

[27] Yang, D., Huang, S.S., Liu, F., et al. “Structural fire design of square tubed-reinforced-concrete columns with connection to RC beams in composite frames”, *Journal of Building Engineering,* 57, pp. 104900 (2022),

[28] Li, Z., Ding, F., Cheng, S., et al. “Mechanical behavior of steel-concrete interface and composite column for circular CFST in fire”, *Journal of Constructional Steel Research*, 196, pp. 107424 (2022).

[29] Bouzoubaâ, N., and Lachemi, M. “Self-compacting concrete incorporating high volumes of class F fly ash: Preliminary results”, *Cement and Concrete Research,* **31**(3), pp. 413-420 (2001).

[30] Okamura, H., and Ouchi, M. “Self-compacting concrete”, *Journal of Advanced Concrete Technology*, 1, (2003).

[31] ACI-318-19, Building Code Requirements for Structural Concrete and Commentary, Farmington Hills, MI, USA, (2019)

[32] C. ASTM, ASTM standards, Philadelphia: American Society for Testing Materials (1958)

[33] EFNARC, European Federation for Specialist Construction Chemicals and Concrete Systems, United Kingdom, (2005)

[34] ACI-Committee-237, Self-consolidating concrete, ACI 237R-07 Farmington Hills, American Concrete Institute (2007)

[35] Anand, N., and Godwin, A. “Influence of mineral admixtures on mechanical properties of self-compacting concrete under elevated temperature”, *Fire and Materials*, **7**(40), pp. 940-958 (2016).

[36] Aydin, A.C. “Self compactability of high volume hybrid fiber reinforced concrete”, *Construction and Building Materials*, **21**(6), pp. 1149-1154 (2007).

[37] Aydin, A.C., Arslan, A., and Gül, R. “Mesoscale simulation of cement based materials’ time-dependent behavior”, *Computational Materials Science*, **41**(1), pp. 20-26 (2007).

[38] Aydin, A.C., and Bayrak, B. “The torsional behavior of reinforced self-compacting concrete beams”, *Advances in Concrete Construction*, **8**(3), pp. 187-198 (2019).

[39] Aydın, A.C., Kan, A., Candan F., et al. “Sulphate Resistance of Boron Active Belite Cement Concrete”, *Journal of Cement Based Composites*, **1**(1), pp. 11-16 (2020).

[40] Khaloo, A., Raisi, E.M., Hosseini, P., et al. “Mechanical performance of self-compacting concrete reinforced with steel fibers”, *Construction and Building Materials,* 51, pp. 179-186 (2014).

[41] Kurt, M., Gül, M.S., Gül R., et al. “The effect of pumice powder on the self-compactability of pumice aggregate lightweight concrete”, *Construction and Building Materials,* 103, pp. 36-46 (2016).

[42] Uzbaş, B., and Aydın, A.C. “Analysis of fly ash concrete with Scanning Electron Microscopy and X-ray diffraction”, *Advances in Science and Technology*, *Research Journal*, **13**(4), (2019)

[43] ISO-834, Fire Resistance Tests, Elements of Building Construction, International Standards Organization (1980)

[44] Xiong, M.X., and Liew, J.R. “Mechanical behaviour of ultra-high strength concrete at elevated temperatures and fire resistance of ultra-high strength concrete filled steel tubes”, *Materials & Design*, 104, pp. 414-427, (2016).

[45] Chan, S.Y.N., Luo, X., and Sun, W. “Effect of high temperature and cooling regimes on the compressive strength and pore properties of high performance concrete”, *Construction and Building Materials,* **14**(5), pp. 261-266 (2000).

[46] Li, M., Qian, C., and Sun, W. “Mechanical properties of high-strength concrete after fire”, *Cement and Concrete Research,* **34**(6), pp. 1001-1005 (2004).

[47] Tao, J., Yuan, Y., and Taerwe, L. “Compressive strength of self-compacting concrete during high-temperature exposure”, *Journal of Materials in Civil Engineering,* **22**(10), pp. 1005-1011 (2010).

[48] Bai, J., Wild, S., and Sabir, B. “Sorptivity and strength of air-cured and water-cured PC–PFA–MK concrete and the influence of binder composition on carbonation depth”, *Cement and Concrete Research,* **32**(11), pp. 1813-1821 (2002).

[49] Emmanuel, A.O., Oladipo, F.A., and Olabode, O. “Investigation of salinity effect on compressive strength of reinforced concrete”, *Journal of Sustainable Development,* **5**(6), pp. 74-82 (2012).

[50] Mohamed, H.A. “Effect of fly ash and silica fume on compressive strength of self-compacting concrete under different curing conditions”, *Ain Shams Engineering Journal*, **2**(2), pp. 79-86 (2011).

[51] Raheem, A.A., Soyingbe, A.A., and Emenike, A.J. “Effect of curing methods on density and compressive strength of concrete”, *International Journal of Applied Science and Technology*, **3**(4), (2013)

[52] ASTM-C109, Standard test method for compressive strength of hydraulic cement., American Society for Testing and Materials (1992)

[53] ASTM-E8, Standard Test Methods for Tension Testing of Metallic Materials, (2016)

[54] Atienza, J., and Elices, M. “Behavior of prestressing steels after a simulated fire: Fire-induced damages”, *Construction and Building Materials*, **23**(8), pp. 2932-2940 (2009).

[55] Ding, F., Zhang, C., Yu Y., et al. “Hysteretic behavior of post fire structural steels under cyclic loading”, *Journal of Constructional Steel Research*, 167, pp. 105847 (2020)

[56] Huang, L., Li, G.Q., Wang, X.X., et al. “High temperature mechanical properties of high strength structural steels Q550, Q690 and Q890”, *Fire Technology*, **54**(6), pp. 1609-1628 (2018).

[57] Kelly, F., and Sha, W. “A comparison of the mechanical properties of fire-resistant and S275 structural steels”, *Journal of Constructional Steel Research,* **50**(3), pp. 223-233 (1999).

[58] Morozov, Y.D., Chevskaya, O., Filippov, G., et al. “Fire-resistant structural steels”, *Metallurgist,* **51**(7), pp. 356-366 (2007).

[59] Xiao, J., Xie, Z., Li, Xie, Q., et al. “Effect of strain rate on compressive behaviour of high-strength concrete after exposure to elevated temperatures”, *Fire Safety Journal*, 83, pp. 25-37 (2016).

Biographies

Abdulkadir Cüneyt Aydın is professor in Civil Engineering Department at Atatürk University. His research interest includes structural engineering, steel structures, performance of constructed facilities, repair and strengthening in building, masonry structures, building materials, composite materials, material mechanics. He is also Editor-in-Chief of the Journal of Cement Based Composites, Brilliant Engineering, Civil Engineering Beyond Limits and member of the editorial board and a reviewer of many journals, academic societies.

Barış Bayrak received Master and PhD degrees from Ataturk University, Erzurum, Turkey. He is member of Civil Engineering Department at Kafkas University at Kars. His research focuses on structural engineering.

Haluk Görkem Alcan is faculity member of Kafkas University at Kars. He is PhD candidate at Ataturk University, Erzurum, Turkey. His research is mainly concentrated on material technology.

Mahmut Kılıç is received his BSc, Master and PhD degrees in Civil Engineering from Ataturk University, Erzurum, Turkey. He is currently an Associate Professor at the Civil Engineering Department, Ataturk University. His research interests include structural engineering, steel structure and engineering technology.

Mahyar Maali completed his PhD from Civil Engineering Department from Ataturk University. He has published many research papers in national and international conferences and journals.

LIST OF CAPTIONS

Figure Captions

Table Captions

FIGURES

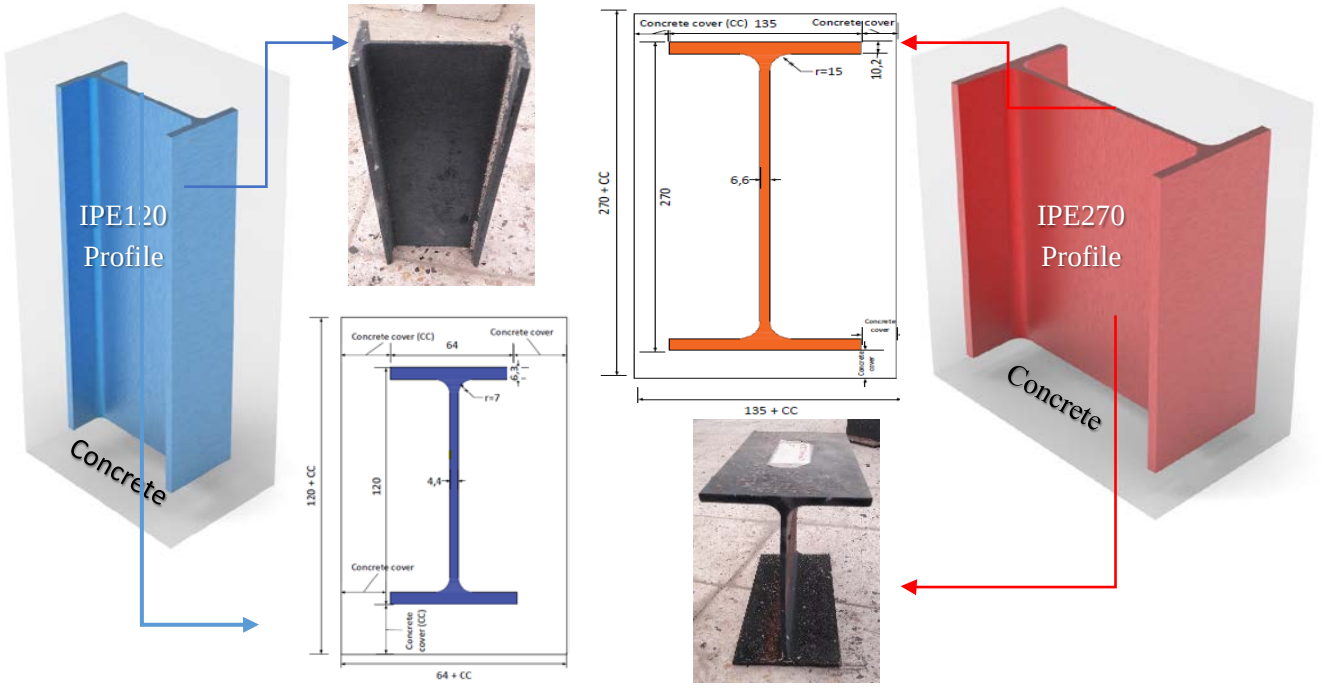

Figure 1. The geometrical details of specimens

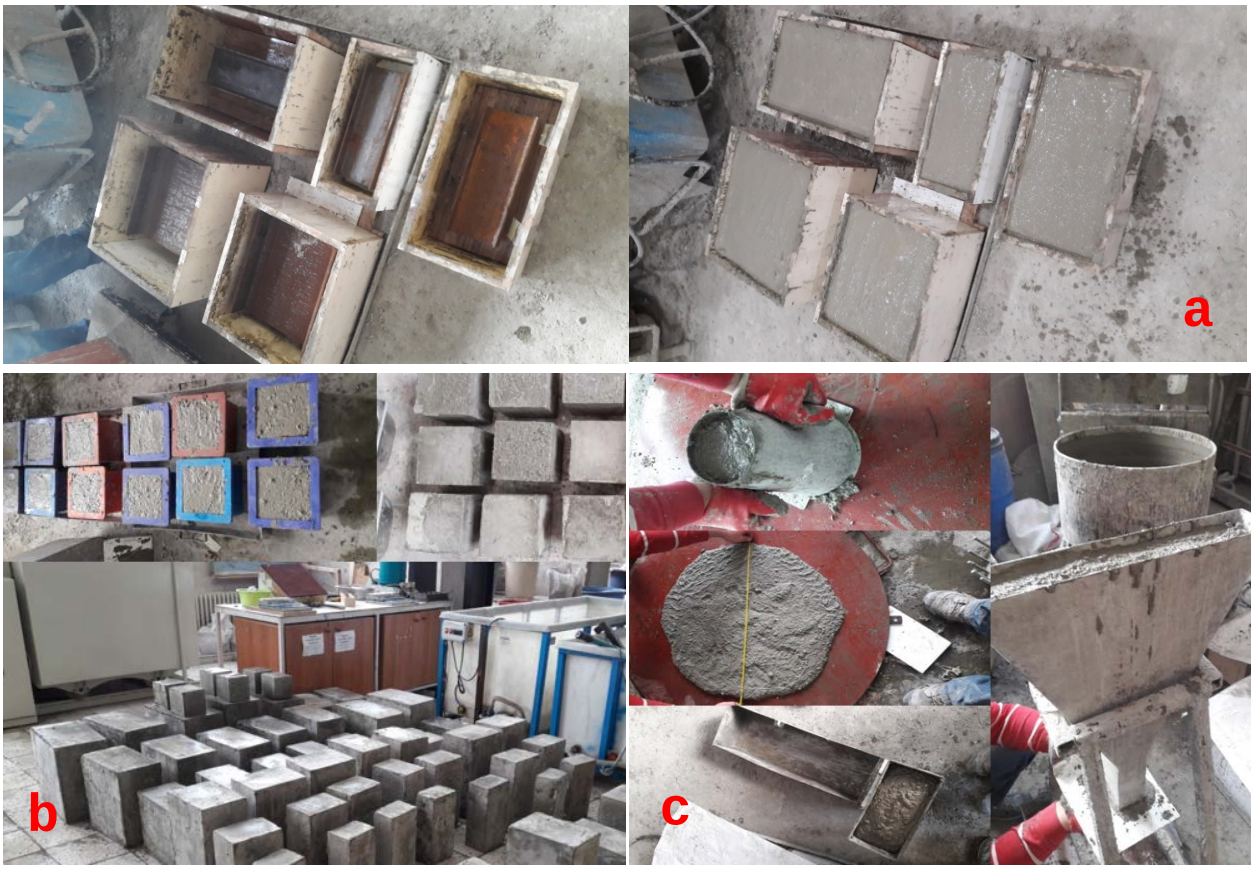

Figure 2. The production phase of specimens a) fresh concrete b) hardened concre specimens c) L-box and V-funnel tests

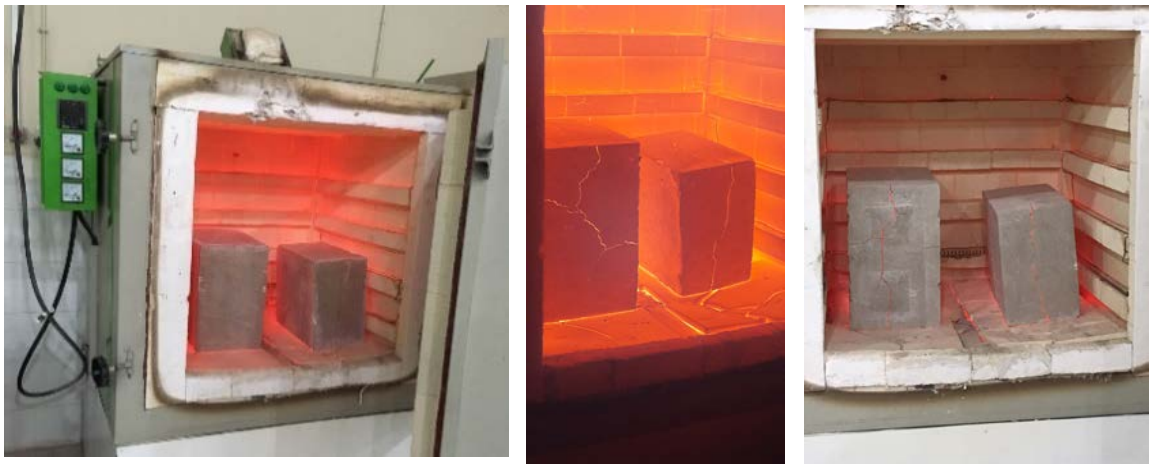

Figure 3. High temperature furnace at the structural laboratory

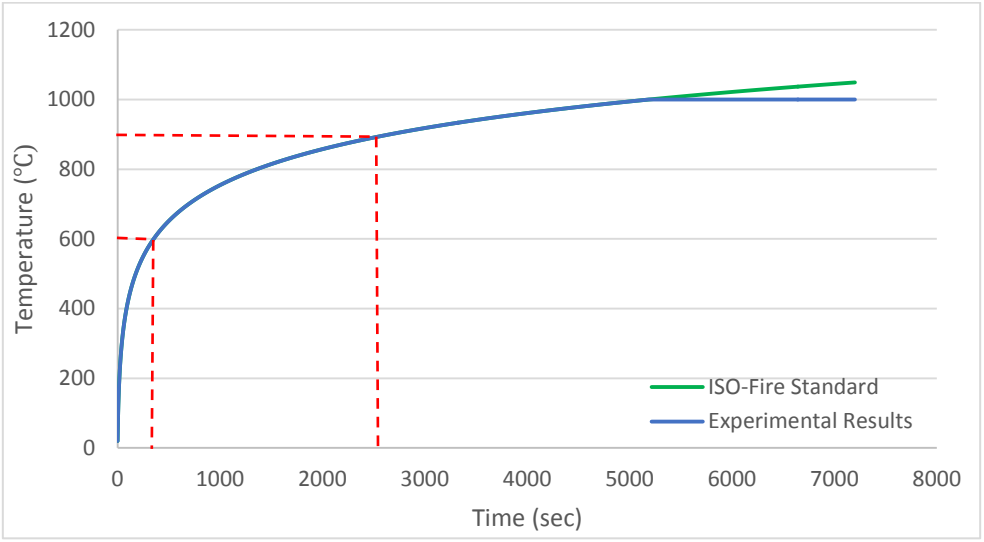

Figure 4. ISO standard and experimental temperature-time curves

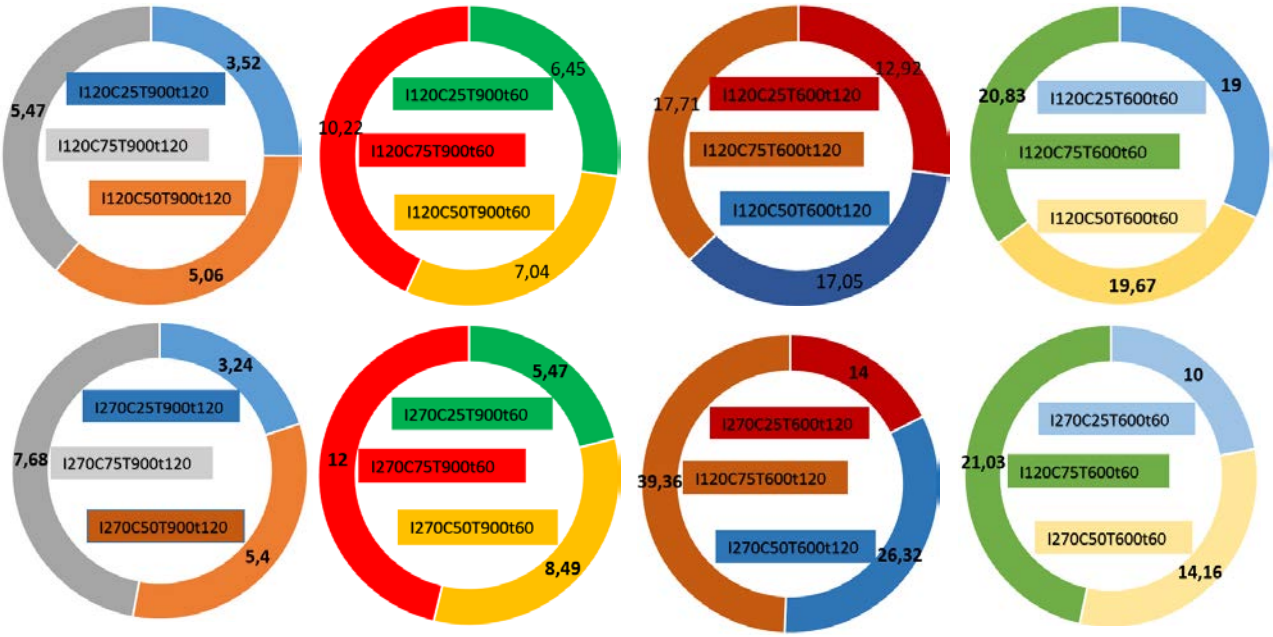

Figure 5. The effect of concrete cover, temperature and exposed time on the compressive strength (All units are MPa)

Figure 6. The photos of samples before and after tensile test

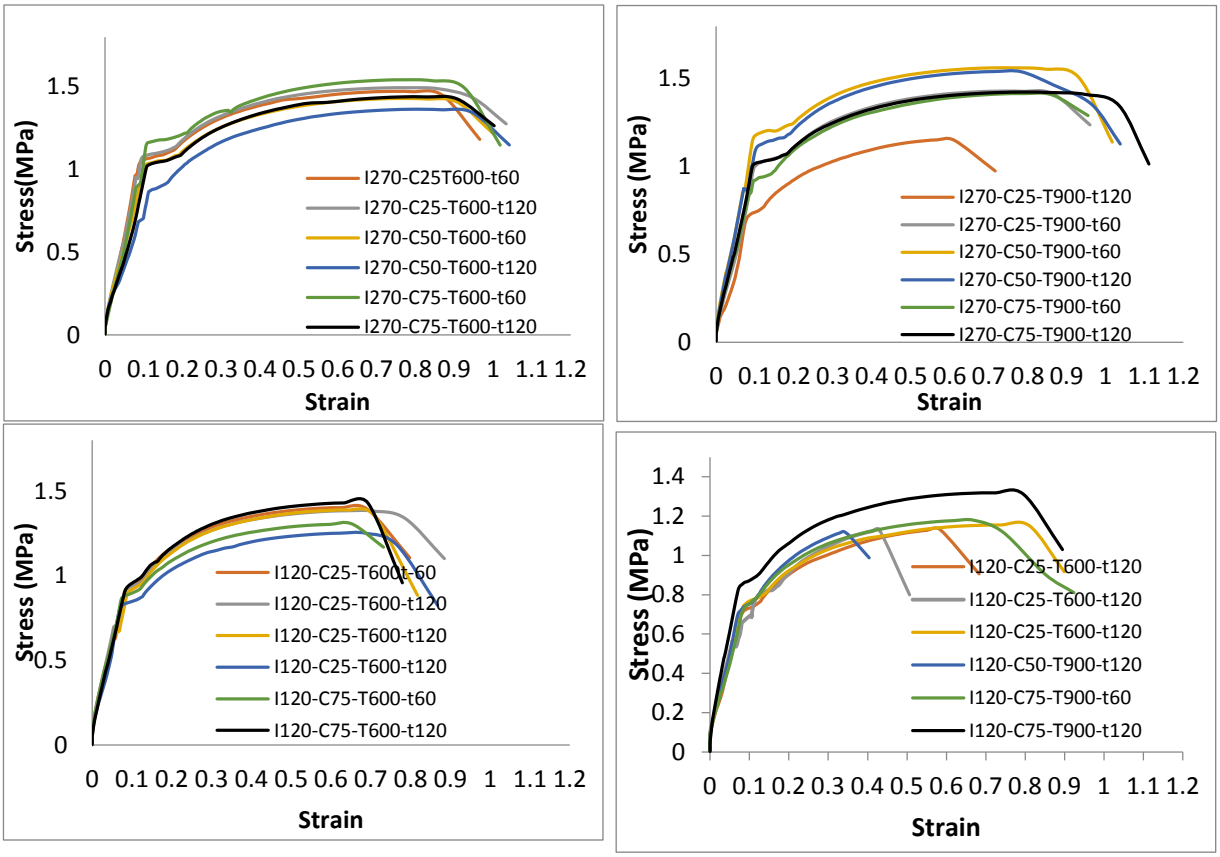

Figure 7. Stress-strain curves of the samples

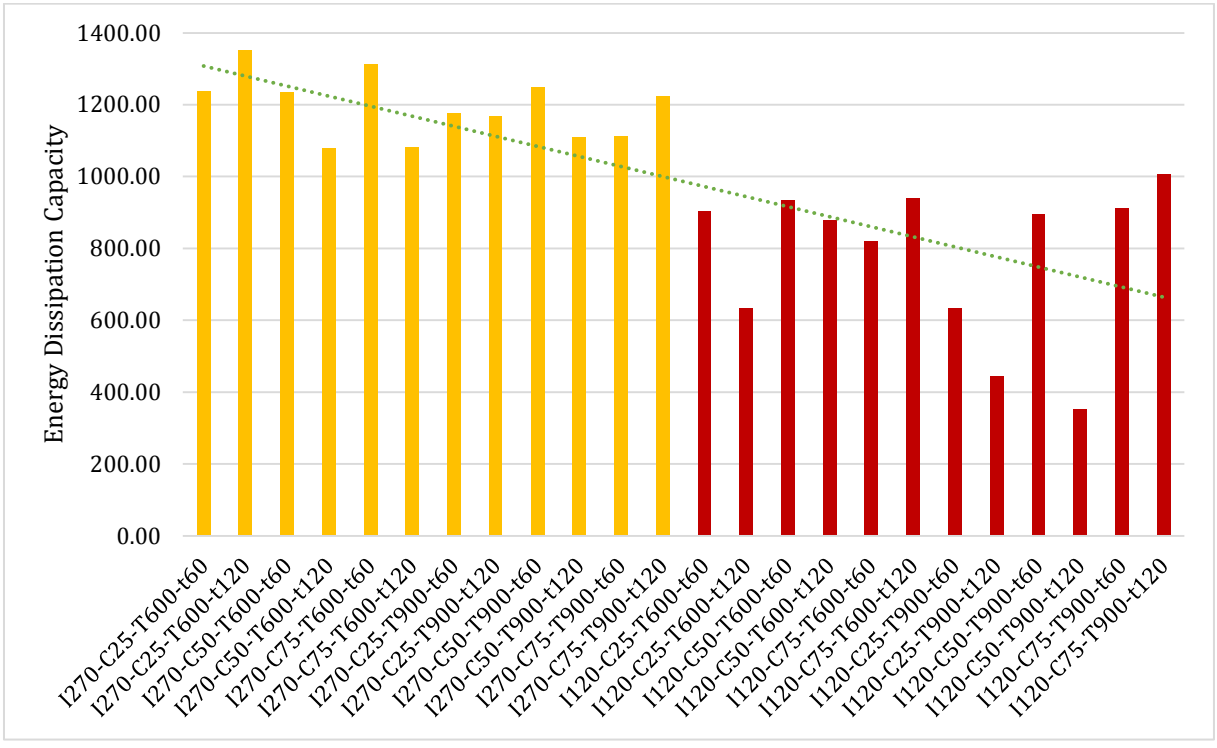

Figure 8. The energy dissipation capacity of samples

Figure 9. Crack propagation of specimens a) I120 group b) I270 group

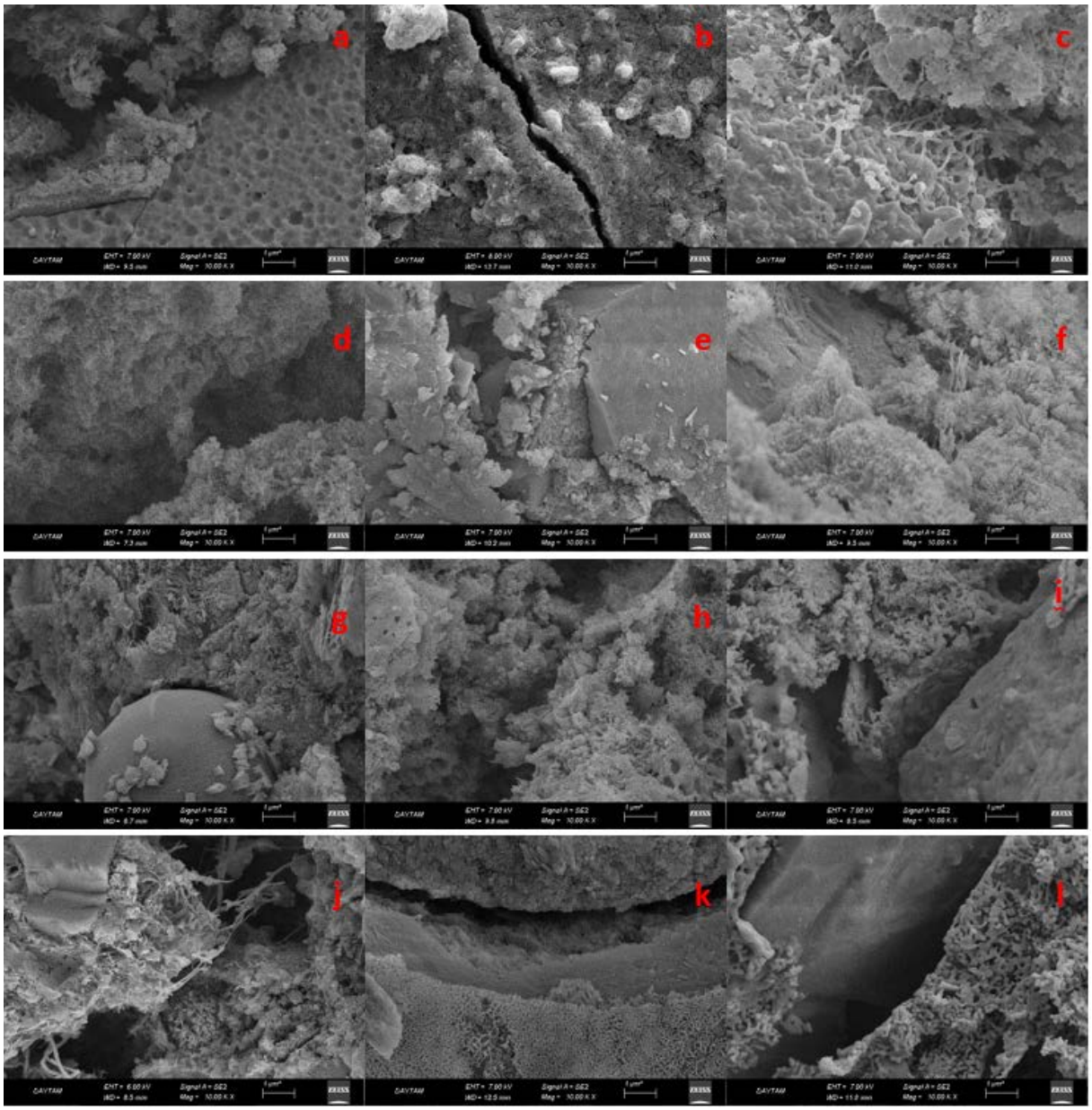

Figure 10. The SEM images of the thermal-processed concrete samples a) AC-T600-t60 b) AC-T600-t120 c) AC-T900-t120 d) I120-C25-T600-t120 e) I120-C50-T600-t120 f) I120-C75-T600-t120 g) I270-C50-T600-t120 h) I270-C50-T900-t60 i) I270-C25-T900-t60 j) WC-T600-t60 k) WC-T600-t120 l) WC-T900-t120
(AC: Air cured; WC: Water cured, for concrete only samples)

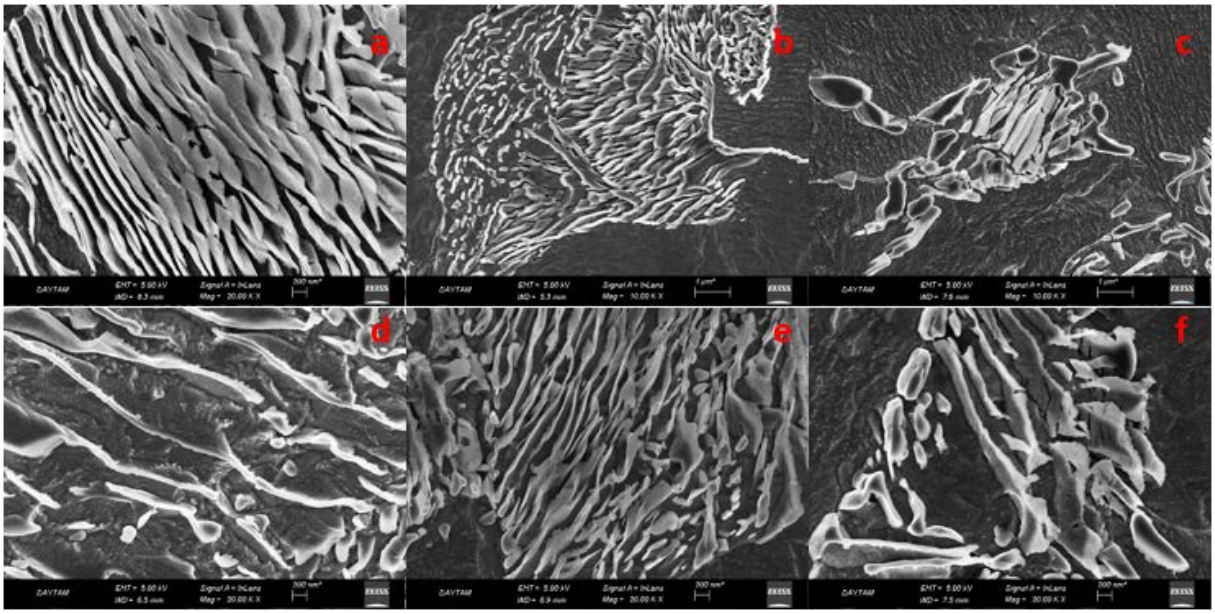

Figure 11. The SEM images of the thermal-processed samples from profiles within the composite
a) I120-C25-T600-t120 b) I120-C25-T900-t120 c) I120-C75-T900-t120
d) I120-C25-T600-t60 e) I270-C50-T900-t120 f) I270-C75-T900-t120

TABLES

Table 1. Details of the experiments and the specimens

Group	Specimens	Time (min)	Concrete cover (mm)	Temperature (degree)	Cross-section (mm)
I270	I270-C25-T600-t60	60	25	600	185x320x350
	I270-C25-T600-t120	120	25	600	
	I270-C50-T600-t60	60	50	600	235x370x400
	I270-C50-T600-t120	120	50	600	
	I270-C75-T600-t60	60	75	600	285x420x450
	I270-C75-T600-t120	120	75	600	
	I270-C25-T900-t60	60	25	900	185x320x350
	I270-C25-T900-t120	120	25	900	
	I270-C50-T900-t60	60	50	900	235x370x400
	I270-C50-T900-t120	120	50	900	
	I270-C75-T900-t60	60	75	900	285x420x450
	I270-C75-T900-t120	120	75	900	
I120	I120-C25-T600-t60	60	25	600	114x170x350
	I120-C25-T600-t120	120	25	600	
	I120-C50-T600-t60	60	50	600	164x220x400
	I120-C50-T600-t120	120	50	600	
	I120-C75-T600-t60	60	75	600	214x270x450
	I120-C75-T600-t120	120	75	600	
	I120-C25-T900-t60	60	25	900	114x170x350
	I120-C25-T900-t120	120	25	900	
	I120-C50-T900-t60	60	50	900	164x220x400
	I120-C50-T900-t120	120	50	900	
	I120-C75-T900-t60	60	75	900	214x270x450
	I120-C75-T900-t120	120	75	900	

Table 2. Chemical properties of Portland cement and fly ash

	Chemical properties								Physical properties	
	SiO_2	Al_2O_3	Fe_2O_3	CaO	MgO	SO_3	Na_2O	K_2O	Specific gravity (g/cm^3)	Specific surface (cm^2/g)
Cement	18.11	4.60	2.96	64.49	2.34	2.95	0.13	0.66	3.15	3954
Fly Ash	47.15	20.42	4.15	20.47	1.51	2.08	0.59	1.36	2.20	2986

Table 3. The concrete mixture

w/c	Cement (kg/m^3)	Fly ash (kg/m^3)	Water (kg/m^3)	Fine aggregate (kg/m^3)	Coarse aggregate (kg/m^3)	Superplasticizer (kg/m^3)
0.37	468	83	192	863	640	11

Table 4. Results of the L-box and V-funnel tests

Slump flow (mm)	L-box	Funnel (s)
710	0.16	1.98

Table 5. The compressive strength (90^{th} day) of the cube sample

Specimens	Compressive strength air cured (MPa)	Compressive strength water cured (MPa)
T900 t120	2.80	4.00
T900 t60	3.60	5.00
T600 t120	13.30	20.70
T600 t60	13.60	21.00
Control Sample	18.38	30.80

Table 6. The compressive strength (90th day) of specimens

Specimens (I270 group)	Compressive strength air cured (MPa)			Specimens (I120 group)	Compressive strength air cured (MPa)		
	C25	C50	C75		C25	C50	C75
T900- t120	3.24	5.40	7.68	T900- t120	3.52	5.06	5.47
T900- t60	5.47	8.49	12.00	T900-t60	6.45	7.04	10.22
T600- t120	14.00	26.32	39.36	T600-t120	12.92	17.05	17.71
T600- t60	10.00	14.16	21.03	T600-t60	19.00	19.67	20.83

Table 7. Average characteristic values for structural steels

Sample	E (MPa)	f_y (MPa)	f_u(MPa)	$\rho_y = f_y/f_u$	ε_y	ε_u
I270-C25-T600-t60	12.12	1.05	1.47	0.71	0.67	0.09
I270-C25-T600-t120	11.72	1.97	1.49	1.32	0.71	0.09
I270-C50-T600-t60	11.42	1.02	1.43	0.71	0.75	0.10
I270-C50-T600-t120	8.570	0.86	1.35	0.64	0.69	0.11
I270-C75-T600-t60	10.73	1.15	1.53	0.75	0.71	0.11
I270-C75-T600-t120	8.860	1.02	1.43	0.71	0.76	0.11
I270-C25-T900-t60	9.960	1.01	1.42	0.71	0.72	0.10
I270-C25-T900-t120	8.880	0.71	1.15	0.62	0.56	0.08
I270-C50-T900-t60	13.30	1.17	1.56	0.75	0.71	0.09
I270-C50-T900-t120	12.89	1.10	1.59	0.69	0.70	0.10
I270-C75-T900-t60	9.950	0.93	1.41	0.66	0.73	0.11
I270-C75-T900-t120	9.450	1.01	1.42	0.71	0.72	0.09
I120-C25-T600-t60	11.16	0.91	1.39	0.65	0.57	0.08
I120-C25-T600-t120	9.900	0.72	1.12	0.64	0.51	0.08
I120-C50-T600-t60	12.04	0.90	1.38	0.65	0.59	0.09
I120-C50-T600-t120	11.30	0.83	1.24	0.67	0.57	0.07
I120-C75-T600-t60	12.38	0.87	1.29	0.67	0.55	0.07
I120-C75-T600-t120	11.65	0.93	1.41	0.66	0.55	0.09
I120-C25-T900-t60	9.900	0.72	1.12	0.64	0.51	0.08
I120-C25-T900-t120	11.11	0.56	1.10	0.51	0.38	0.05
I120-C50-T900-t60	9.460	0.76	1.14	0.67	0.62	0.09
I120-C50-T900-t120	10.47	0.69	1.12	0.62	0.34	0.07
I120-C75-T900-t60	9.400	0.72	1.17	0.62	0.61	0.08
I120-C75-T900-t120	14.59	0.85	1.35	0.63	0.61	0.08